Molecular dynamics simulations of weak detonations

Morag Am-Shallem,[1] Yehuda Zeiri,[2,3] Sergey V. Zybin,[4] and Ronnie Kosloff[1]
[1]*Fritz Haber Research Center, Hebrew University, Jerusalem 91904, Israel*
[2]*Department of Biomedical Engineering, Ben-Gurion University, Beer-Sheva 84105, Israel*
[3]*Chemistry Department, NRCN, P.O. Box 9001, Beer-Sheva 84190, Israel*
[4]*Materials and Process Simulation Center, California Institute of Technology, Pasadena, California 91125, USA*
(Received 13 June 2011; revised manuscript received 31 October 2011; published 12 December 2011)

Detonation of a three-dimensional reactive nonisotropic molecular crystal is modeled using molecular dynamics simulations. The detonation process is initiated by an impulse, followed by the creation of a stable fast reactive shock wave. The terminal shock velocity is independent of the initiation conditions. Further analysis shows supersonic propagation decoupled from the dynamics of the decomposed material left behind the shock front. The dependence of the shock velocity on crystal nonlinear compressibility resembles solitary behavior. These properties categorize the phenomena as a weak detonation. The dependence of the detonation wave on microscopic potential parameters was investigated. An increase in detonation velocity with the reaction exothermicity reaching a saturation value is observed. In all other respects the model crystal exhibits typical properties of a molecular crystal.

DOI: 10.1103/PhysRevE.84.061122 PACS number(s): 47.40.Rs, 62.50.Ef, 82.40.Fp

I. INTRODUCTION

Explosives are characterized by a detonation wave which propagates through the material. After initiation, the velocity of the detonation front reaches a steady state that exceeds the speed of sound in the material. The present paper is devoted to the analysis of a model solid explosive with the purpose of correlating the microscopic structure and interatomic forces to the bulk detonation properties. The investigation is based on a classical molecular dynamics simulation with a simple force field. The initial goal was to construct a first-principle model that is able to qualitatively reproduce a stable detonation wave. The microscopic parameters considered are the crystal structure, the intermolecular forces that stabilize this structure, and the intramolecular potentials that yield the driving chemical reaction. The present investigation unravelled a new type of a solitary-like detonation wave that is directly driven by the one-step exothermic chemical decomposition. From a hydrodynamical perspective it can be classified as a weak detonation.

A common theoretical framework for simulating detonations relies on a continuum picture of the material properties using a hydrodynamic description and is based on the conservation of mass, momentum, and energy [1–4].

In the Chapman-Jouguet (CJ) model, the detonation wave is considered as a discontinuity between "unburnt" and "burnt" material, assuming that the transition from one state to another does occur instantaneously. It assumes an infinite reaction rate and requires only the knowledge of the thermodynamic equilibrium state of the burnt material to satisfy the conservation relations on the Hugoniot curve of compressed detonation products. The resulting detonation wave has zero-width reaction zone and should satisfy the minimum entropy solution of the Rankine-Hugoniot equations, which corresponds to *sonic condition* for downstream flow (downstream velocity with respect to the front, which equals the isentropic sound speed in reacted material). Freely propagating one-dimensional (1D) detonation wave without the piston (*unsupported detonation*) attains the steady-state velocity satisfying the sonic condition. The CJ model is used extensively as an engineering tool enabling quick calculation of the detonation velocity and pressure in the design of explosive devices.

An extension of the CJ model was proposed by Zel'dovich, von Neumann, and Döring [5–7] (ZND) that incorporates finite-rate reaction kinetics resulting in a chemical reaction zone of finite length. It assumes that the unreacted explosive material behind the front is initially compressed to a high pressure resulting in a so-called von Neumann pressure spike. Then the chemical reactions are initiated behind the spike, leading to the exothermic energy release, temperature increase, and expansion of the reaction products to the lower pressure. The structure and length of the reaction zone is determined by the equation of state of intermediate products. After completion of the reactions, the products reach the final equilibrium state, at the end of the reaction zone. The final state determines the detonation velocity and depends only on the equation of state of the reaction products. For an unsupported detonation wave, this state satisfies the sonic condition as in the CJ model and is called the CJ state.

In the ZND model, besides the minimum-entropy (or, correspondingly, minimum-velocity) solution to the conservation equations, there are two other possible detonation propagation regimes. In a case of piston-supported detonation, the downstream flow can be subsonic in respect to the front and is called *strong or overdriven detonation*. Another type of possible hydrodynamical solutions is termed weak detonation. It is characterized by a downstream flow behind the detonation front that is supersonic in respect to the burnt material and effectively *decouples* from it (i.e., no disturbances from the burnt material can overtake the front). In addition, the weak detonation wave is characterized by only a moderate increase in density and pressure, which is smaller than the CJ pressure on the detonation products Hugoniot.

Zel'dovich [8] stresses that the weak detonation solution satisfies the boundary conditions of shock propagation and therefore is an admissible hydrodynamical solution. He argues that the reason that the weak detonation phenomenon has

not been observed experimentally is the unattainability of the steady-state conditions of this solution. In particular, a typical ZND route from the unreacted shock-compressed state to the burnt material gets trapped in the stable CJ point of minimum entropy production. Von Neumann, however, has shown that if the Hugoniot curves of partially reacted products intersect, then the weak detonation solution is possible [6]. For example, explosives that have very rapid initial exothermic decomposition followed by a slower endothermic reaction may exhibit such behavior, sometimes called *pathological detonation*. It has been also speculated by Tarver, based on a hydrodynamical equations, that in porous materials weak detonation could be stable [9]. Though standard ZND model assumes that chemical reactions are triggered by the high temperature due to the initial shock compression, it is also possible to consider an alternate ignition mechanism without preliminary shock heating at the von Neumann spike. Zel'dovich [10] discussed possible initiation of weak detonation by triggering chemical reactions with a sequence of sparks artificially fired along a tube.

Can a first-principle molecular dynamics (MD) simulation converge to the hydrodynamical detonation model?

There has been a continuous effort to develop MD simulation methods of explosives [11,12]. An interaction potential, known as the Reactive Empirical Bond Order potential (REBO), was introduced in Ref. [13]. This potential has a complex functional form and several parameters. Molecular dynamics simulations of detonation through a model two-dimensional (2D) crystal using this potential showed agreement with the predictions of the CJ model [14].

A significant step was the development of a reactive force field that accounts for breaking and forming chemical bonds during the passage of the shock wave through the solid [15]. Simulations of actual explosives, such as RDX, PETN, and TATP, have been attempted [16–23]. The main goal is to compare the simulation output to known experimental characteristics of the system, such as detonation velocity and final reaction products distributions. These studies were devoted to establish a realistic simulation scheme that converges to the framework of the hydrodynamic models. It was found that the goal of reaching steady-state detonation conditions requires a major computational effort. The phenomenon stabilizes only in a mezoscopic scale (micrometers), which requires very large-scale calculations including many millions of atoms. To establish such a method as a predictive tool, many such simulations should be performed and compared with experiment. A second round of improvements should then be applied to the force field. At present, this task is still in its infancy.

Schemes to bridge the gap between the hydrodynamical description of detonation and the MD approach have been explored. The idea is to replace a group of molecules by a single mesoparticle with an internal thermodynamic degree of freedom [24,25] or to describe a hydrodynamical cell by fictitious particles [26]. In both these schemes individual molecular properties are overlooked.

In the present study a different MD approach was utilized. We limited the objective to establish a relationship between the forces governing the dynamics in the microscopic system and the macroscopic phenomena. The simple molecular force field employed is constructed to have only a small number of adjustable parameters. In a three-dimensional (3D) model, we observed stable detonation waves, their characteristics being independent of the initial conditions. It required a more thorough investigation to identify that these detonation waves are of a different character from those in the standard ZND model.

A first indication of a new phenomenon can be inferred from the 1D model of Peyrard *et al.* [27], constructed from a chain of unstable diatomic molecules. The dissociation reaction generated an accelerating detonation wave. In order to obtain a stable detonation wave artificial dissipation channels were added. Our analysis of their model revealed that a detonation wave in the 1D chain resembles a solitary wave. Further understanding requires a full 3D crystal model that should supply a natural dissipative mechanism.

The initiation of detonation wave in solids is closely related to the propagation of a shock wave through a crystal lattice. Both waves are quasi-1D. Early MD simulations of a planar shock wave in a perfect fcc crystal [28,29] revealed the formation of a solitary-like train at the shock front over a wide range of shock velocities. It has oscillatory structure and exhibits significant deviation from the thermal equilibrium inside the train. In addition, the MD simulations of shocks in a perfect bcc crystal have shown [30] that an isolated solitary wave can be emitted from the shock front and run ahead it at significantly faster speed than the shock front velocity. This links the present study to the subject of solitary waves propagation in a discrete lattice. Solitons are characterized by a group velocity that is proportional to the amplitude of the wave. For a 1D lattice we refer to the work of Toda, who established a relationship between the microscopic parameter of the repulsive part of the potential and the group velocity [31,32]. Holian has performed MD simulations of shock waves in the 1D Toda lattice to study the dependence of solitary train structure at the shock front on the interaction potential parameters [33].

Can the energy release reaction occur directly at the shock front as in the CJ model? The prerequisite is a metastable molecule whose one-step exothermic decomposition is triggered by the shock front, and its energy is immediately fed back into the detonation wave. By definition, shock wave propagation is faster than any linear elastic wave in the same material. As a result it will always confront *fresh* unperturbed molecules. For these molecules to contribute to the detonation event, their initial decomposition time scale should be similar or faster than the time scale determined by the front propagation velocity. Slower processes can take place behind the shock front. These processes may include thermal equilibration and heat dissipation as well as slower chemical reactions that lead to the final product distribution. If the slower reactions are endothermic, the weak detonation wave can be initiated.

In the present study we identified a diatomic molecule where the exothermic decomposition is sufficiently fast and can proceed directly at the detonation front. We observed a propagation of fast supersonic reactive wave initiated by the impulse impact in a 3D perfect molecular crystal. We analyze the dependence of the detonation wave parameters on the interaction potential and the molecule decomposition

kinetics. We find that the downstream flow is supersonic, and the density increase behind the front is very small, which is typical for a weak detonation. We also observe the decoupling of supersonic front propagation from the dissipative dynamics of the decomposed material left behind the front. Our analysis suggests that the weak detonation wave in the simulated crystal resembles behavior of a solitary wave propagating at the supersonic speed through the lattice. The molecule decomposition is triggered at the detonation front where a significant thermal nonequilibrium exists. The released energy is directly channelled into acceleration of the atoms from the dissociated molecules pushing solitary detonation front forward. Remarkably, the front propagation dynamics significantly depends on the relative orientation of the light and heavy atoms in the molecule with respect to the shock direction.

The simulation results show a possibility of fast initiation of the molecule decomposition reactions at the supersonic solitary wave front in contrast to the standard ZND model where the reactions take place behind the shock front, initiated by the shock compression. Summarizing, the solitary front ignition can provide a mechanism for a direct transition to the weak detonation regime from the initial uncompressed state without going first to the high-pressure state by the shock compression.

II. THE COMPUTATIONAL MODEL

An explosive is defined as a molecular crystal that can decompose to smaller particles, generating a stable detonation wave. The front of the detonation wave moves faster than the speed of the linear compression wave in the molecular crystal. MD simulation of detonations requires a scheme of molecular forces, initial geometry, boundary conditions, and atomic masses. The model should be able to sustain a stable crystal structure. Simulation of the system is based on the solution of the classical equations of motion with sufficient accuracy, using a modified version of the MD code MOLDY, which is described in Appendix A.

A. The reactive molecule model

The model crystal is represented by a slab of diatomic molecules arranged in a crystal structure. Each of the atoms can represent also a group of atoms. The two effective particles will be marked as N and C, and the masses are 47 amu for N and 15 for C. These notations and masses originated from nitromethane: the N corresponds to the NO_2 group, and the C to the CH_3 group. The difference between the masses is essential in such reactive molecular model [27]. However, no other similarity to nitromethane exists in our model. The chemical bond between N and C is designed to be metastable. When energized it can dissociate exothermally. The shape of the potential energy curve as a function of the N-C distance is shown in Fig. 1. When the distance N-C is smaller than the barrier position the molecule is bound. However, when this distance is increased beyond this position the molecule disintegrates. In an energetic perspective, the molecule absorbs sufficient energy such that its internal energy is higher than the energy barrier. Separation of the N-C atoms results in

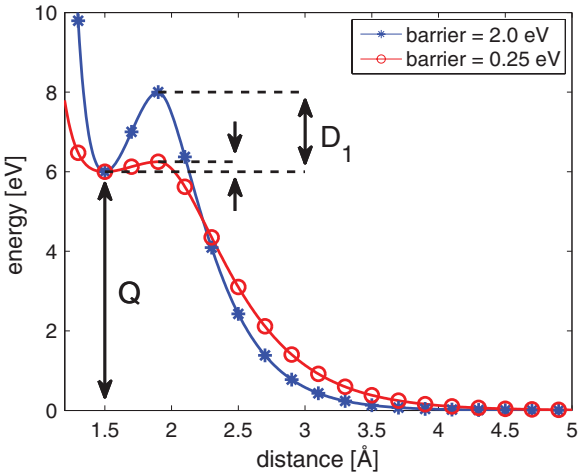

FIG. 1. (Color online) The reactive internal potential as a function of the N-C distance for two different ratios between the barrier height and the exothermicity. When the distance N-C is smaller than the barrier position (here at 1.9 Å, the local maximum) the molecule is bound. When the distance is increased beyond this position the molecule dissociates. Initially the N-C distance is at the equilibrium distance (here at 1.5 Å, the local minimum). Q represents the exothermicity, and D_1 the barrier height for the N-C dissociation.

decomposition of the molecule to its constituents accompanied by energy release. The evaluation of the potential and force during the trajectory calculations was carried out by generating and storing a table of the potential and force values at different N-C distances, according to the potential shown in Fig. 1, or similar potentials. A cubic spline interpolation was used to extract the values. There are functional forms that can be used to generate such an exothermic reactive potential; some of them are described in Ref. [11]. We used a piecewise defined function to generate the potential; its functional forms are described in Appendix B.

B. The molecular crystal

The molecular crystal was constructed by a lattice of N-C molecules with a bonding interaction between similar groups in neighboring molecules. The N entity interacts with other N and C interacts with other C entities. A Morse potential was chosen to describe these interactions:

$$V(r) = D(e^{-2\beta(r-r_0)} - 2e^{-\beta(r-r_0)}). \quad (1)$$

The parameters used are shown in Table I. The initial distances between nearest neighbor molecules was chosen as $r_0 = 7.5$Å. A long and narrow slab of this molecular crystal was assembled with FCC symmetry. Other structures studied, the BCC and simple cubic crystals, were found to be unstable with this type of pair potentials. This finding is consistent with analysis of stability of Lennard-Jones crystals [34].

C. Boundary conditions and initial conditions

We expect the detonation wave to be quasi-1D Hence, the reactive crystal slab used is chosen to be long and narrow. The direction of the propagation axis was chosen as Z, and it coincides with the [111] crystallographic axis. The molecular

TABLE I. Potential parameters used for the intermolecular interaction. The third line shows the parameters of the inner part of the intramolecular reactive bonding potential (see Appendix B). The same potentials were used for N-C atoms of different molecules.

Interaction	D (eV)	β (Å^{-1})	r_0 (Å)
N-N	0.08	1.0	7.5
C-C	0.016	1.0	7.5
N-C (inner part):			
Barrier of 0.25 eV	0.25	4.33	1.5
Barrier of 2.0 eV	2.0	4.33	1.5

axes were also oriented along the Z direction. Thus, the crystal is very nonisotropic. The length of the periodic unit in the [111] direction of an FCC crystal is $\sqrt{6}$ times r_0. In our case $r_0 = 7.5$Å, so the length of the periodic unit is ≈ 18.37Å. This distance will be referred to in the following as the unit cell length. The length of the crystal was 295 unit cells along the Z direction, and, in some cases, a crystal with a length of 587 unit cells was used. Periodic boundary conditions were imposed along the perpendicular directions X and Y. To check that the size of the cross section is sufficient we ran simulations of crystals with various cross sections. It was found that detonation properties are converged in the larger cross sections. The converged cross section that was eventually used consists of 48 molecules in the XY plane.

The shock wave was initiated by a small crystal pellet, assigned with an initial high velocity in the Z direction. The pellet collided with one of the small faces (XY plane) of the slab. The velocity of the pellet was not kept constant: The MD simulations were of *NVE* type, and the positions and velocities of the pellet's particles were calculated with no distinction. The pellet was composed of three crystal layers along the Z direction and had 48 N-C molecules in each layer. The collision of this pellet was sufficient to initiate a sustainable shock in the primary crystal.

Most of the simulations were carried with initial temperature of 0 °K. A few simulations were carried with higher initial temperatures.

III. WEAK DETONATION WAVES IN THE CRYSTAL

The analysis of weak detonation wave starts from the static properties of the reactive crystal. The second step describes the initiation process, showing that a stationary detonation wave is formed, independent of initiation process. The classification as a weak detonation relies on thermodynamics analysis of the phenomena.

The equilibrium properties of the crystal model were characterized. The details are summarized in Appendix C. A linear relation was found between the velocity of the elastic p-wave and the stiffness of the potential [the β parameter in Eq. (1)].

A. Initiation of stable detonation waves

We ran *NVE* simulations of shock waves in the model reactive crystal, initiated by the small pellet described above. After initiating a shock wave, a transient emerges, eventually stabilizing into a stable shock front. Such simulations were run with different crystal parameters and different initial velocities of the pellet. The propagating shock wave initiated a decomposition reaction in crystals composed of reactive molecules. When the decomposition reaction kept pace with the shock front, the shock wave transformed into a detonation wave. The simulations were carried with initial temperature of 0 °K. A few simulations were carried with higher initial temperatures, in order to verify that the phenomenon is not restricted to 0 °K.

A stable detonation wave is independent of initial conditions. This was verified by using different initial pellet velocities leading to shock waves that are independent of these initial velocities. The details can be found in Appendix D, and in Fig. 17.

A snapshot of the detonation process is shown in Fig. 2. A distinction between the unperturbed crystal and the burnt material is clearly seen. An enlarged section of the reaction zone is shown on the bottom.

Similar simulations, with an endothermic intramolecular Morse potential, yielded decaying shock waves, with propagation velocity that depends on the initial pellet velocity.

B. Classification of the detonation waves as weak detonations

After the short transient the shock wave stabilized into a stable weak detonation wave. The shock front propagated in a very high Mach number, practically decoupled from other processes in the crystal. The number of molecules that were decomposed by this shock front changed from one simulation to another, depending on internal potential parameters such as the exothermicity and the barrier height for C-N dissociation. Only a small compression was associated with this front. Other properties, such as the mass velocity (see Sec. III C 2) and the kinetic energy (see Sec. III C 3), also exhibit an increase in magnitude. This shock wave will be referred to as the reaction wave in the following.

The reaction wave travels through an unperturbed crystal, and therefore its velocity is determined by the crystal properties (see Sec. IV). The reaction wave propagation velocity, as well as its amplitude, are independent of the initial impact (see Appendix D). The velocity does depend on the exothermicity of the reaction, which is an intrinsic property of the material. The dependence of the detonation velocity on the reaction exothermicity will be discussed later (see Sec. IV A).

After the reaction wave, another shock front appeared, characterized by a large increase of both the mass velocity and the kinetic energy. In the second shock front most of the remaining molecules dissociated, leading to a decomposition yield of above 85%. This second shock wave will be referred to as the compression wave in the following. In contrast to the reaction wave, the amplitude of the compression wave decays during its propagation. The compression wave velocity depends on the impact strength but not on the exothermicity.

The reaction wave is faster than the compression wave: $u_{\text{reaction}} > u_{\text{compression}}$ (see Figs. 3 and 4). *This fact categorizes the reaction wave as a weak detonation:* The compression wave is a typical shock wave. It moves faster than sound waves in the reacted material; therefore it sets an upper limit for the sound wave velocity: $u_{\text{compression}} > u_{\text{sound}}$. Thus,

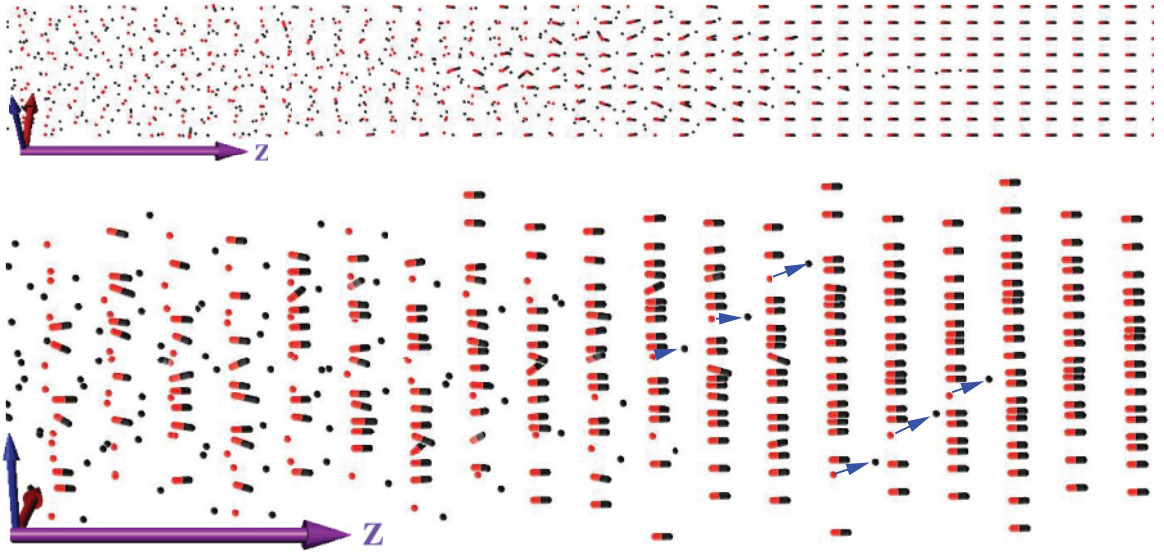

FIG. 2. (Color online) A snapshot of the detonation wave. The propagation axis is the Z direction. Periodic boundary condition are used in the X, Y directions. The right-hand side shows the unperturbed crystal structure. The red (gray) objects represent the heavy particles (N). The black objects represent the light particles (C). On the left-hand side of the image one can observe the burnt material after the passage of the shock wave. The shock front is characterized by pilot cascades of light particles that are emitted from the decomposed molecules and initiate the next layer in a domino-like effect. The lower panel is an enlarged viewpoint of the detonation front. The arrows indicate decomposed N-C pairs, corresponding to the pilot cascade. This simulation was carried out with exothermicity of 6 eV and a barrier of 0.25 eV. Eventually, in this simulation, in approximately 20 layers, most of the material is decomposed.

$u_{\text{reaction}} > u_{\text{sound}}$. We see that the reaction wave is supersonic with respect to the matter behind it. This is the hydrodynamical definition of weak detonation [4 p. 280].

C. Thermodynamics profiles of the weak detonation waves

The profiles of weak detonations differ from those of normal detonations: In weak detonations there is no compression of the material before the reaction. After the reaction front, there is only a small change in the density, pressure, and velocity of the particles.

1. Different dissociation barrier height

Figure 3 compares the decomposition fraction of two simulations as a function of time and position. The first corresponds to molecules that have an N-C dissociation barrier of 2 eV (left plot). The second corresponds to molecules with a dissociation barrier height of 0.25 eV. The reaction exothermicity in both simulations is 6 eV. For a dissociation barrier of 2 eV, ∼35% of the molecules are decomposed by the reaction wave. When the compression wave passes through the partially "burnt" material, most of the remaining molecules decompose (small fluctuations around 90%). For a smaller dissociation barrier, 0.25 eV, more than 85% of the molecules are decomposed simultaneously with the *reaction* shock front.

The reaction wave velocities are almost independent of the dissociation barrier height, as can be seen in Fig. 3. The barrier does influence the mass velocity and the decomposition fraction. The decoupling of the reaction wave from the compression wave and from the dissociation process results from the fact that this is the fastest wave in the material, leaving behind the slower processes. This phenomenon is another signature of a weak detonation wave.

2. Mass velocity profile

The mass velocity characterizes the mass current and is defined as $\langle v \rangle = \frac{\sum_i m_i v_i}{\sum_i m_i}$. Figure 4 shows a contour plot of the Z component of the mass velocity during the simulation. The mass velocity plot shown can be compared to the decomposition percentage during the same simulation (right-hand side of Fig. 3): The decomposition front and the discontinuity of the mass velocity coincide, and define the reaction wave. The compression wave is observed on the mass velocity plot, but is absent from decomposition plot since the majority of the molecules have already decomposed.

Figure 5 shows profiles of mass velocity at different snapshots during the simulation. The values were averaged over bins with a constant number of particles, 96, in each bin. The top plot shows the Z component of the mass velocity along the solid for three time values. The largest amplitude (the left peak for each time) is associated with the compression wave. At later times the peak mass velocity decays due to dissipation. The first shock front (the right sudden change in velocity for each time) is associated with the reaction wave. The insert shows a zoom-in on the reaction fronts. The average mass velocity after the reaction front, ∼0.3 km/s, is much smaller than the reaction front velocity, ∼65 km/s. This is consistent with a small increase of density after the reaction front (see Fig. 8). It is clear that the reaction wave amplitude does not decay. When comparing simulations with different parameters, we find that the reaction wave amplitude depends on the reaction exothermicity and is independent of the impact strength. As

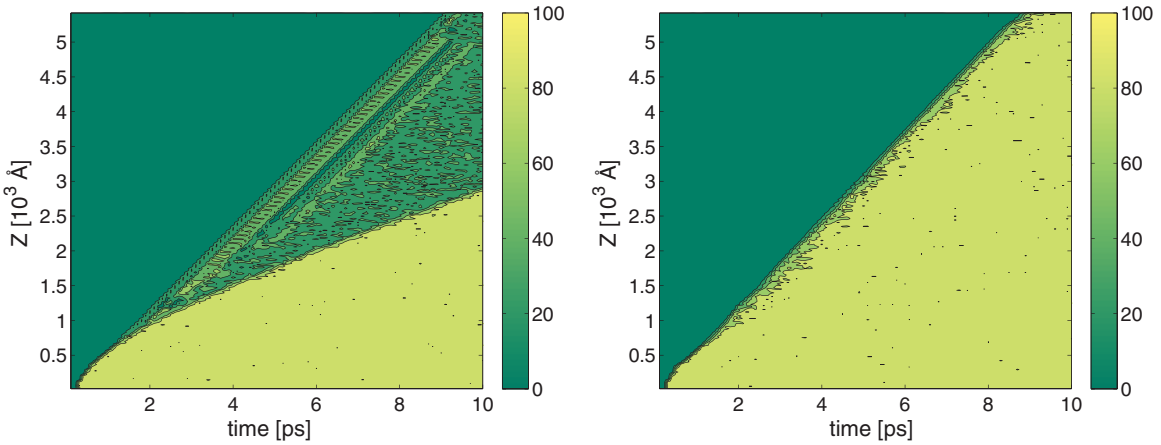

FIG. 3. (Color online) Contour plots of decomposition percentage during two different simulations. The left plot is obtained in a simulation with a dissociation barrier of 2 eV. Some of the molecules are decomposed by the reaction wave. Most of the other molecules (around 90%) are decomposed by the compression wave. The right plot is obtained in a simulation with a decreased dissociation barrier of 0.25 eV. More than 85% of the molecules are decomposed by the reaction wave. In both cases the exothermicity is 6 eV, and the initiating pellet velocity is ~90 km/s. The reaction front velocity in the case of the higher barrier, ~60 km/s, is very similar to the case of the smaller one, ~62.5 km/s.

discussed above, in the Introduction and in Appendix D, this is a characteristic of a detonation wave. The compression wave behaves differently: It has a decaying amplitude that does not depend on the exothermicity but does depend on the impact strength. The compression wave is a regular compression shock wave. It travels through an unstructured matter composed of reaction decomposition products.

The X component of the mass velocity is shown in the bottom plot for a single snapshot. The shock front is characterized with a abrupt onset of fluctuations. There is a minor change after the first shock front.

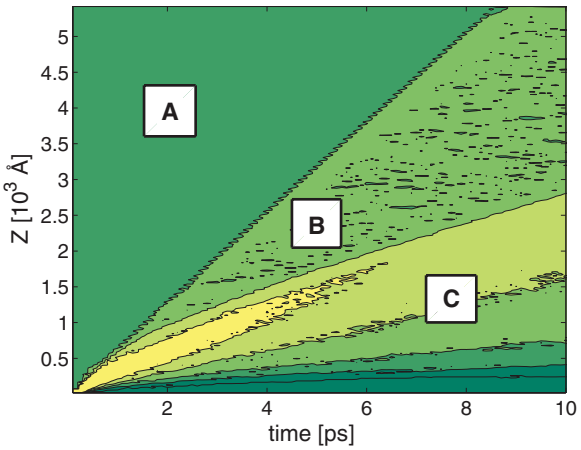

FIG. 4. (Color online) Contour plot of mass velocity along the Z direction. The dissociation barrier height in this simulation was 0.25 eV, and the reaction exothermicity was 6 eV. The initiating pellet velocity was ~90 km/s. Three regions are marked in the plot: Region A is the preshocked material. The mass velocity here is 0. Region B is the material after the reaction wave. The mass velocity here fluctuates around an average value of 0.3 km/s (see Fig. 5 for more detailed profiles). The mass velocity plot shown here can be compared to the decomposition percentage during the same simulation, which is shown on the right plot of Fig. 3: The decomposition front and the discontinuity of the mass velocity coincide, characterizing the reaction wave. Region C is the material after the compression wave. The mass velocity on the peak of the compression wave decays from around 20 km/s at 1 ps to 8.5 km/s at 10 ps. The compression wave is visible on the mass velocity plot but is almost absent on the decomposition plot: For this barrier height, most of the molecules have already decomposed before the compression wave reached them.

3. *Energies and temperature*

Further insight on the detonation process can be obtained by inspection of the kinetic energy and the local temperature profiles, shown in Figs. 6 and 7, respectively. The profiles correspond to an intermediate time of 10 ps. The local temperature is defined as $T_l = \frac{1}{Nk_B}\sum_i^N m_i\,(v_i - \langle v\rangle)^2$, where $\langle v\rangle$ is the mass velocity defined above. The values were determined by averaging over bins with a constant (96) number of particles. The reaction wave front can clearly be seen as a sharp change in kinetic energy and temperature. The insert in the local temperature figure shows a small region after the first shock front, which is not thermalized. The increase of the Z component of the local temperature precedes the corresponding increase of the X component.

Figure 8 shows the potential energy and the density profiles at the same time step. On the right, a small increase of the potential energy is observed, followed by a large decrease. The small increase is caused by a minor compression before the dissociation starts, as seen in the density profile. The large decrease that follows is caused by the energy release of the exothermic decomposition process. The average density after the reaction front is only slightly larger than the density before this front. This is consistent with the small increase in the mass velocity (see Fig. 5). This phenomenon characterizes weak detonations.

IV. SATURATION OF THE WEAK DETONATION VELOCITY

The detonation wave can be characterized by a stable detonation velocity independent of initiation parameters, as

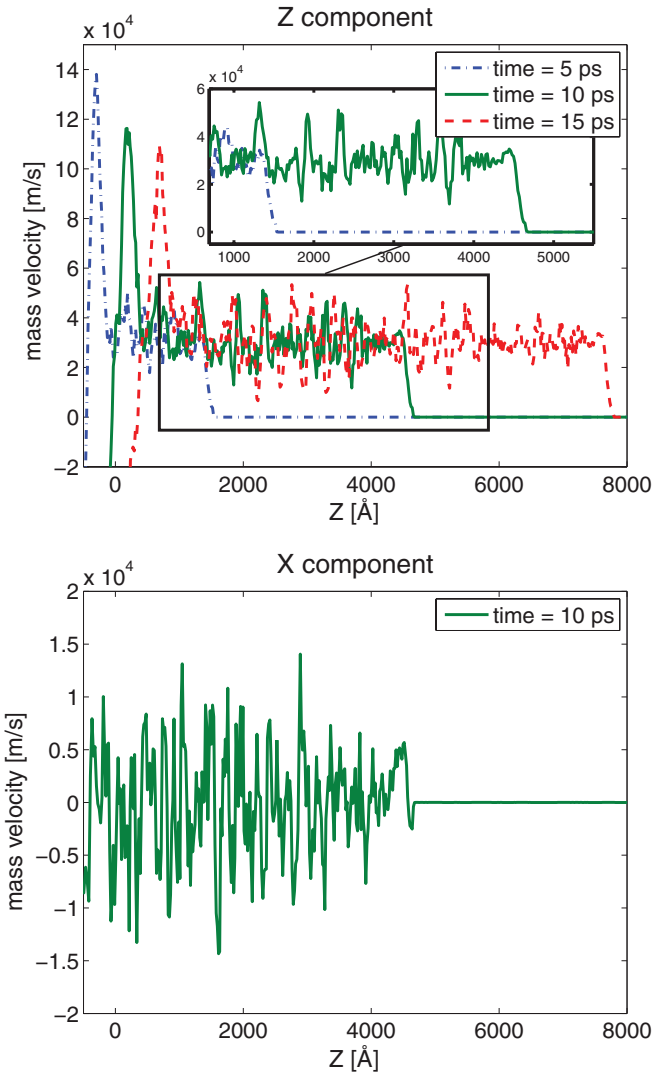

FIG. 5. (Color online) Mass velocity profiles along Z and X directions. The exothermicity of the reaction in this simulation was 6 eV, and the barrier was 0.25 eV. The values were determined by averaging over bins with constant 96 particles in each bin. The left edge of the crystal is placed at -500Å. The top plot shows the profile of the mass velocity in the Z direction, at three time values. The bottom plot presents the mass velocity along the X direction at a single time value. Along the Z direction (top figure), the largest amplitude (the left peak on each time step) is associated with the secondary compression wave. At later times the peak mass velocity decays due to dissipation. The first shock front (the right peak on each time step) is associated with the reaction wave. The reaction wave amplitude does not decay. The insert shows a zoom of the first shock fronts for the two shorter times. The average mass velocity after the reaction front, $\sim$0.3 km/s, is much smaller than the reaction front velocity, $\sim$65 km/s.

discussed in Appendix D. The terminal velocity of the wave is a function of the microscopic parameters used in the model. Insight aimed at deciphering the phenomena is obtained by a systematic study of the variation of the detonation velocity as a function of the parameters of interest.

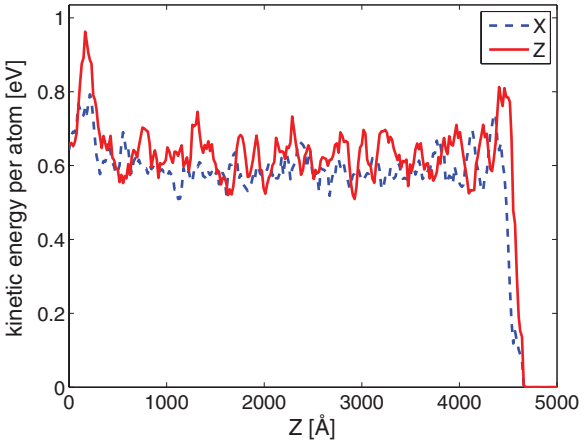

FIG. 6. (Color online) Normalized kinetic energy profile at time $=$ 10 ps. The exothermicity of the reaction in this simulation was 6 eV, and the dissociation barrier was 0.25 eV. The values were averaged over bins with constant number of particles, 96, in each bin. The blue dashed line corresponds to kinetic energy along the Xdirection, and the red solid line to kinetic energy along the Z direction. The large peak on the right corresponds to the reaction wave front.

A. Intramolecular potential parameters: Exothermicity of the reaction

Simulations of detonation using reactive slabs were carried out with different values of the exothermicity. All other parameters, such as crystal structure, impact magnitude, intermolecular potential, particles masses, initial conditions, were kept constant. Figure 9 displays the reaction propagation, which is determined by the dissociation front, in crystals with different exothermicity values. In the exothermicity range displayed in

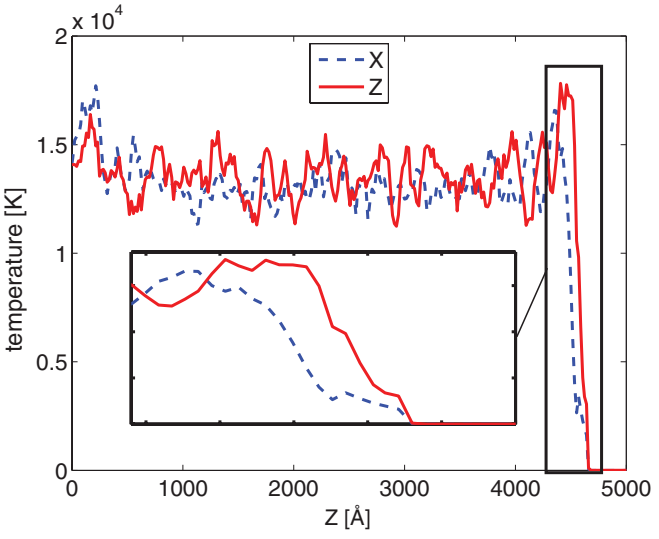

FIG. 7. (Color online) Local temperature profile at time $=$ 10 ps. The parameters are the same as in Fig. 6. The blue dashed line represents temperature along the X direction, and the red solid line along the Z direction. The insert shows an unthermalized region: The large peak on the right is the reaction wave front. The increase of the Z component of the local temperature precedes the increase of the X direction.

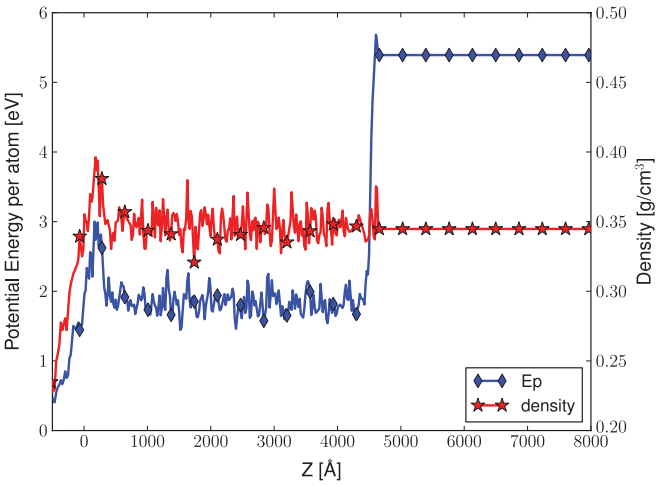

FIG. 8. (Color online) Potential energy (E_p) and density profiles at $t = 10$ ps. The parameters are the same as in Fig. 6. The first shock front displays a small increase of the potential energy, due to a small compression before the dissociation. This small increase is followed by a large decrease of the potential energy, due to the energy release of the exothermic decomposition. The average density after the reaction front is not significant higher than the density before this front. The peak on the left is associated with the compression wave.

the figure (1.0–3.5 eV), the detonation velocity increases as a function of exothermicity. At larger exothermicity values, the detonation velocity reaches saturation: Simulations with exothermicity values above 3.0 eV show only a minor increase in the detonation velocity. Figure 10 displays the variation in detonation velocity as a function of reaction exothermicity. The kinetic energy of the particles behind the reaction wave was found to depend linearly on the exothermicity of the reaction. Thus it is responsible for the energy balance. Nevertheless, in weak detonations this additional kinetic energy is decoupled from the reaction shock front.

The saturation effect is an interplay between three factors: the crystal rigidity, responsible for the nonlinear wave propagation, shear effects, responsible for energy dissipation at the reactive shock front, and kinematic effects, which determine

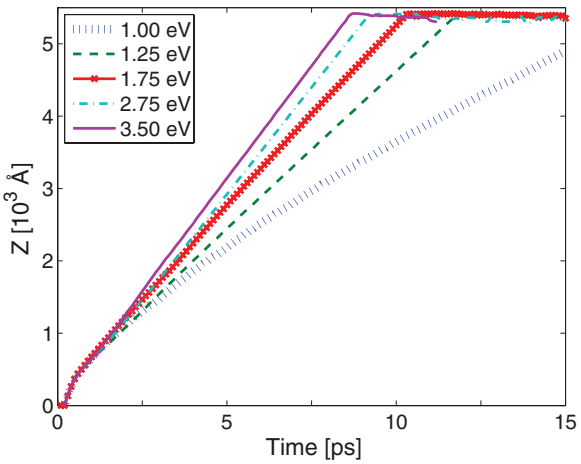

FIG. 9. (Color online) Reaction front propagation in crystals with different exothermicity values. All other parameters are identical.

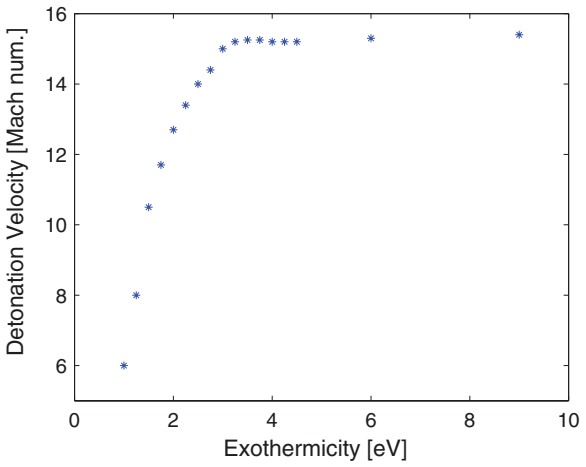

FIG. 10. (Color online) Detonation velocity in the crystal as a function of reaction exothermicity. The detonation velocity is measured in reduced units, normalized to the p-wave velocity, which is 4.6 km/s. We can see the increase of detonation velocity as a function of exothermicity at low exothermicity values, until approximately 3 eV. The saturation of the detonation velocity at high exothermicity values can also be seen. The saturation was verified by simulations with very high exothermicity values: There is a very small increase of the detonation velocity in crystals with higher exothermicity values (12, 15, 18, and even 27 eV; these results are not shown here).

the partitioning of the energy release during the decomposition of a single molecule.

Some insight regarding kinematic effects and the crystal rigidity is discussed in the following; see Secs. IV B and IV C. The nonlinear effect of shear was not explored systematically in this study. The convergence of the calculations was checked to an increase in the XY cross section (see Sec. II C). While checking convergence, we found that increasing the cross section decreases the detonation velocity. This is an indirect indication that the detonation velocity is sensitive to shear.

B. Kinematic effects

In weak detonations the decomposition mechanism of the reactive molecules has to be linked to the characteristics of the detonation wave. A propagation by a domino-like effect, as seen in Fig. 2, requires the decomposition to be asymmetric with respect to the Z direction. Insight is obtained by examining a simplified 1D model of decomposition of a single diatomic molecule. Initially the molecule is at rest. A light particle emerges from the decomposition of the neighboring molecule and hits the molecule from the heavier side (Fig. 11, top). The collision initiates the decomposition process. At the end of the decomposition, the light particle of this molecule is emitted toward the next molecule (Fig. 11, bottom). The mass of the light particle is denoted by m, and the mass of the heavier particle is αm ($\alpha > 1$). After the initiation collision, the molecule decomposes, and the heat of the reaction, E, releases as kinetic energy. The velocity of the colliding particle is denoted by v_1. After the decomposition, the velocities are denoted by u_1, u_2, u_3, for the colliding particle, the heavy particle, and the light particle, respectively.

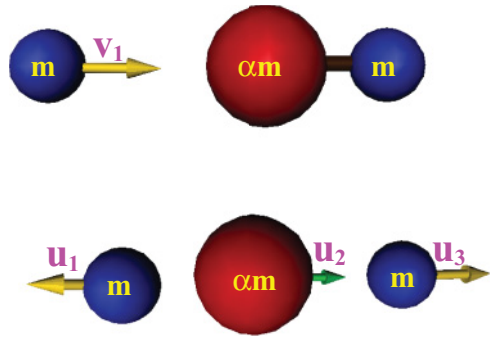

FIG. 11. (Color online) A molecule is hit by a light particle, emitted from neighboring decomposition (top diagram). After the collision, the molecule decomposes (bottom diagram).

Under these conditions the equations for momentum and energy conservation become

$$\begin{aligned} mv_1 &= mu_1 + \alpha mu_2 + mu_3, \\ \tfrac{1}{2}mv_1^2 + E &= \tfrac{1}{2}mv_1^2 + \tfrac{1}{2}\alpha mu_2^2 + \tfrac{1}{2}mu_3^2, \end{aligned} \tag{2}$$

where we assume that the collision is complete, meaning that all potential energy has been consumed. In steady-state detonation, the initial velocity of the colliding particle should be equal to the velocity of the emitted light particle:

$$v_1 = u_3, \tag{3}$$

and this should also become the group detonation velocity.

Two mechanisms come to mind: a direct and a delayed decomposition. In the direct decomposition mechanism, Eqs. (2) and (3) give the complete kinematic picture. Substituting Eq. (3) into Eq. (2) cancels out the terms v_1 and u_3. Therefore, the detonation velocity is undetermined without further assumptions. In order to determine the wave propagation velocity, more details on the dissipation mechanism, the crystal structure and the nonlinear properties are needed.

Next, we analyze the delayed decomposition mechanism. This mechanism has two steps: First, the colliding particle has an elastic encounter with the molecule. The molecule after the collision will acquire a velocity of u_{23} and mass of $(\alpha + 1)m$. In the second step, the molecule will dissociate into its components. The equations for momentum and energy conservation of the first step are

$$\begin{aligned} mv_1 &= mu_1 + (\alpha + 1)mu_{23}, \\ \tfrac{1}{2}mv_1^2 &= \tfrac{1}{2}mu_1^2 + \tfrac{1}{2}(\alpha + 1)mu_{23}^2 \end{aligned} \tag{4}$$

And the equations for momentum and energy conservation of the second step are

$$\begin{aligned} (\alpha + 1)mu_{23} &= \alpha mu_2 + mu_3, \\ \tfrac{1}{2}(\alpha + 1)mu_{23}^2 + E &= \tfrac{1}{2}\alpha mu_2^2 + \tfrac{1}{2}mu_3^2. \end{aligned} \tag{5}$$

Again, we require the steady-state condition, Eq. (3). Solving these equations shows that the velocities $v_1 = u_3$, which are equal to the detonation velocity, are proportional to $\sqrt{E/m}$.

A strong detonation process is adequately described by a delayed mechanism, since there is a delay between the compression (which leads to collisions) and the decomposition. The $\sqrt{E/m}$ dependence of the strong detonation velocity is in accordance with the hydrodynamical theory. This $\sqrt{E}$ dependence was obtained in Ref. [35] in MD simulations of detonations in the REBO model and in Ref. [36] in another crystal model. A different result was obtained in an earlier study [37], in which a linear dependence of the detonation velocity on the energy released is reported.

A weak detonation process is adequately described by the direct mechanism since the reaction coincides with the shock front. In weak detonations, we find the detonation velocity to saturate, becoming independent of the energy release. This means that in our 1D model, only the results of a direct decomposition mechanism can fit this phenomenon. The relation of direct reaction mechanism to weak detonations was shown also in hydrodynamic analysis of the ignition stage [38].

The mechanism discussed above suggests a difference between the two possible reaction wave propagation directions: Different behavior is expected if the reaction wave emits the heavier particle of the molecule, which in turn collides with the lighter particle of the neighboring molecule. This anisotropic behavior of the reaction wave was examined by initiating the shock wave in the opposite edge, impacting from the lighter side of the molecules. Under these conditions, no stable constant velocity reaction waves were formed.

The dependence of the detonation wave velocity on the mass of the emitted particle was also examined. We performed simulations of detonations where the mass of the lighter particle was varied while maintaining the same structure and force field. In order to keep the total mass unchanged, the mass of the heavier particle was also changed. The masses used were 22, 10, and 5 amu for the C particle (and 40, 52, and 57 amu for N, respectively). Several simulations were performed, with different exothermicity values. We expect that decreasing the mass of the C lighter particle will result in a higher velocity, hence faster detonation. This has been already suggested by Peyrard *et al.* [27] in a 1D model. The magnitude of exothermicity at which the detonation velocity saturated was found in all cases to be close to 3 eV. However, the saturation velocity depended on the mass of the emitted C particle. Lower mass of this particle led to an increased detonation velocity. These results are presented in Fig. 12, in log-log scale. A linear fit to the velocity logarithm as a function of the mass logarithm was calculated and is displayed in the graph. The resulting slope is close to 0.5 (0.49), which reveals a $1/\sqrt{m}$ dependence of the detonation velocity on the mass of the emitted group. This dependence is identical to the dependence of the shock velocity of solitons in a Toda lattice.

C. Crystal rigidity: Intermolecular potential parameters

Simulations of the propagation of small amplitude displacements in the crystal showed that the elastic p-wave velocity depends linearly on the β parameter of the intermolecular Morse potential Eq. (1), i.e., the stiffness. This is in agreement with the propagation of elastic waves in a 1D crystal model. See Appendix C2b and Fig. 16 for details.

The shock wave velocity is crucially dependent on the rigidity of the crystal, which is determined by β. To explore this dependence we carried out simulations of detonations in

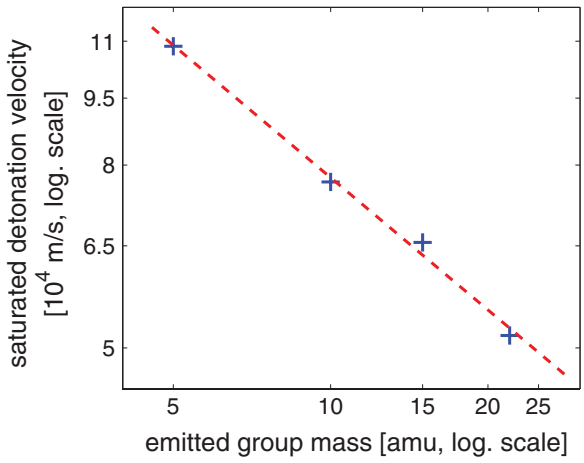

FIG. 12. (Color online) Saturation values of detonation velocities, marked with asterisks, as a function of the mass of the emitted C group. The graph is plotted in logarithmic scale on both axis. In all cases this saturation value is obtained when the exothermicity is close to 3 eV. A linear fit of the data in the log-log scale is also plotted. The slope of the linear fit is close to -0.5 (-0.49), indicating that the detonation velocity is proportional to $1/\sqrt{m}$.

crystals with different β values. The first effect observed is that an increase in β leads to an increase in magnitude of the exothermicity for which the saturated reaction wave velocity is observed. The second effect found is that the saturation reaction wave velocity increased exponentially as a function of β. Figure 13 shows the logarithm of the saturated reaction wave velocity as a function of β. The exponential dependence can be clearly seen. The exponential dependence suggests that the saturation of the reaction wave velocity depends on the repulsive part of the intermolecular potential. This is different from the elastic p-wave velocity, which is governed by the

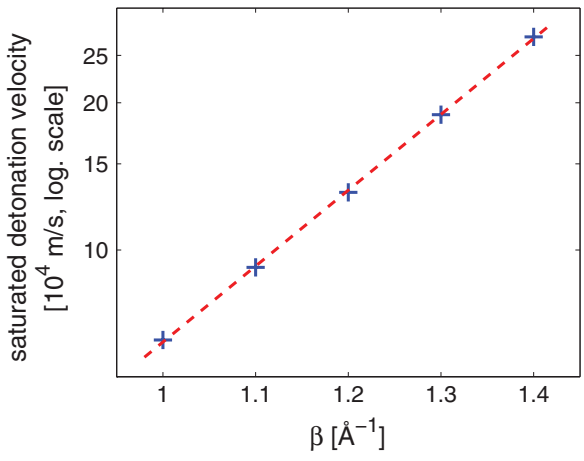

FIG. 13. (Color online) Comparison of reaction propagation velocities (scaled logarithmically) in five different crystals, β ranges from 1 to 1.4 Å^{-1} (when β is the coefficient inside the Morse potential's exponent). The exponential dependence suggests that the saturation of the detonation velocity is caused by the repulsive part of the intermolecular potential. This is different from the elastic p-wave velocity dependence, which is governed by the behavior of the potential near the equilibrium point (see Appendix C2b and Fig. 16).

shape of the potential near equilibrium and varies linearly as a function of β.

To verify that the saturation of the reaction wave velocity is governed by the repulsive part of the intermolecular potential, we ran additional simulations. In these simulations we varied the stiffness of the inner part of the repulsive potential without altering other parameters of the crystal: The potential was combined from a repulsive part of Morse potential with $\beta = 1.2$ Å^{-1} and an attractive part of Morse potential with $\beta = 1.0$ Å^{-1}. The reaction shock wave velocities in these crystals were compared to the previous simulations. We found that the reaction waves velocities were almost identical to those with $\beta = 1.2$ Å^{-1}. To conclude the reactive shock-wave velocity is governed by the repulsive part, and independent of the soft long range part of the potential. This phenomenon characterizes solitary waves, as has been suggested by Toda [31,32] and by Rolfe *et al.* [39].

V. DISCUSSION

The purpose of this study was to bridge the gap between a first-principle microscopic model of detonation and bulk hydrodynamical theories. The first task was to obtain a stable detonation wave independent of initial conditions. For this task we constructed a reactive molecular crystal model characterized by pair potentials. The equilibrium properties of the crystal are typical. It is stable at low temperatures and melts at temperatures that scale with the binding energy. The model crystal also possesses linear elastic waves. The detonation potential was added by making the molecule metastable to dissociation releasing a significant amount of energy. The model fulfilled the expectations and a stable detonation wave was identified.

Further analysis, which compared the results obtained in the simulations to hydrodynamical theory, revealed a puzzling picture. The detonation wave did not have the characteristics of the common solutions of the ZND model. Some of the differences are the following:

(1) The compression at the shock front was minor.
(2) The chemical reaction coincided with the shock front.
(3) The shock velocity was supersonic with respect to the burnt material left behind.

Searching for a meeting point with hydrodynamical theory, we conclude that the phenomenon we observed in the MD simulation is a *weak detonation*. Weak detonation is a possible hydrodynamical solution in which the shock wave is supersonic with respect to the material left behind. The characteristics of weak detonations are different from normal detonations: The weak detonation velocity is higher, and the pressure after completion of the reaction is smaller than in the normal detonation case. Also, in weak detonations there is no compression of the material before the reaction. Zel'dovich argues that such solutions are usually unattainable for substances that are initially inert [8]. However, he points out that weak detonations might occur if the chemical reaction would start in the initial state without preliminary heating of the substance by the shock wave [40]. Dremin states that if self-ignition occurs at a pressure lower than the CJ pressure, a weak detonation wave is observed [41].

Why are weak detonations attainable and stable in our case? The answer is in the kinematic behavior of the crystal. The shock propagates with characteristic of a nonlinear solitary wave. The propagation velocity is determined by the repulsive part of the interatomic potential which is similar to solitons on a Toda lattice. The other kinematic property is the mass of the group that emitted from the dissociating molecule. When the shock front comes from the heavy side, the light particle is breaking out with the majority of the kinetic energy, initiating the reaction on the next crystal plane. This can be imagined as a shock propagation by the domino effect which never looks back. The ideal domino effect has no change in the density after the front. This is accompanied by a negligible increase in the mass velocity. The melting of the crystal and the equilibration of the burnt material lag behind the shock front and are decoupled from it due to the supersonic velocity. Remarkably, when the molecule orientation is the opposite (heavy particle is placed ahead of the light one in the shock direction), then the detonation does not reach a steady state. It explains the details of the solitary wave ignition mechanism. If the light particle is pushed forward at the high (supersonic) velocity after the decomposition, it quickly hits another molecule in the next crystal plane, allowing the reaction to propagate at supersonic speed due to the domino effect. On the contrary, if the heavy particle is placed ahead, it breaks out at much slower velocity, delaying the propagation of the decomposition reaction.

These observations pose additional questions:

(1) What are the conditions that are necessary to observe weak detonation in experiments?

(2) What are the conditions that an MD simulation will reconstruct the standard solutions of the ZND model?

It seems that a prerequisite for a stable weak detonation is a stiff molecular crystal that supports fast propagation of nonlinear shock waves. In addition, the crystal should be very nonisotropic. The molecules are oriented with the light particle pointing toward the propagation direction. We have carried out preliminary simulations with triatomic molecules with similar effects. Anisotropic shock initiation sensitivity has been observed in detonation of explosives composed of single molecular crystals [42]. Recent calculations reveal this anisotropic sensitivity [43,44]. Weak detonations were shown to occur in the shock initiation process in the case of inhomogeneous explosives or inhomogeneous initial conditions [45–47]. Weak detonations in mixtures which have nonmonotonic energy release were shown experimentally [48]. It has been demonstrated that a quasisteady form of weak detonation plays an integral role in describing shock-induced transition to detonation in an explosive material [49]. The transition to normal detonation was shown to occur effectively at the point where the weak detonation slows to the CJ velocity. In cases of very porous materials it can happen that the decomposition wave will remain faster than the compression wave, stabilizing the weak detonation solution [9]. Finally, a weak detonation requires a decomposition reaction which can follow pace with the shock front even at relatively low temperatures. This dictates a time scale of a few tens of femtoseconds.

The prerequisite for the MD simulation to generate the standard results of the Chapman-Jouguet or the more elaborate ZND model is a more complex and slower chemical reaction which can justify the quasi-equilibrium assumption. This influence of the speed and complexity of the reaction can be seen even in 1D models: Elert *et al.* [50] used three-body interaction potentials in a 1D model and got a stable detonation without introducing artificial frictional forces. The studies in Ref. [23] using realistic force fields aim at this direction. Nevertheless, the quasi-equilibrium assumption has been criticized [21]. In the present study we find that most regions of the detonating crystal are well described by quasi-equilibrium assumptions, except the vicinity of the shock front.

ACKNOWLEDGMENTS

We would like to thank Matania Ben-Artzi for insightful and fruitful discussions. We also want to thank Naomi Rom and Ido Schaefer for helpful discussions. The study was partially supported by the Center of Excellence for Explosives Detection, Mitigation and Response, DHS.

APPENDIX A: MOLDY: THE MOLECULAR DYNAMICS PROGRAM

The basic simulation program used to integrate the molecular dynamics equations was MOLDY [51]. MOLDY is suitable for the present purpose due to two primary reasons:

(1) The equations of motion are integrated in MOLDY using a modified version of the Beeman algorithm [51,52]. During detonation simulations there is rapid energy exchange between potential and kinetic energy. Simulations carried out with the Verlet algorithm failed to conserve energy properly. The Beeman algorithm, with higher accuracy in velocities, was found to be adequate.

(2) The neighbor list in MOLDY is built using the linked cell method (see, for example, Ref. [53]). In shock wave simulations the system is not homogeneous: Near the shock front there is a domain with high density, and the common neighbor list algorithm is not efficient for such a situation [11].

Two modifications of the MOLDY code were introduced to fit the requirements of detonation simulations:

(1) MOLDY is constructed to calculate potential energy and forces from a wide set of common analytic potentials. We added an option to calculate the potentials and forces from a pre-prepared stored table, using cubic spline interpolation.

(2) The initial velocities in MOLDY's simulations are sampled from the Maxwell Boltzmann (MB) distribution. The pellet initial velocity were modified so that they could be preassigned, while the velocities of the slab atoms are sampled from the MB distribution.

APPENDIX B: THE FUNCTIONAL FORM OF THE EXOTHERMIC POTENTIAL

The interatomic potential described in Fig. 1 can be constructed by a piecewise defined function, which is composed from three segments, each having a different functional form:

$$V(r) = \begin{cases} D_1(e^{-\beta_1(r-r_{\min})} - 1)^2 + Q & 0 < r < r_{\min} \\ c_3 r^3 + c_2 r^2 + c_1 r + c_0 & r_{\min} < r < r_{\text{bar}} \\ D_2[1 - (e^{-\beta_2(r-r_{\text{bar}})} - 1)^2] & r_{\text{bar}} < r < r_{\text{cut}} \end{cases} \tag{B1}$$

With $r_{\min} = 1.5$ Å, $r_{\text{bar}} = 1.9$ Å, and $r_{\text{cut}} = 7$ Å refer to the positions of the local minimum, the barrier, and the cutoff, respectively. $D_1 = 0.25$ eV is the energy barrier height, Q is the energy release during decomposition of the molecule (the exothermicity of the reaction), and D_2 should satisfy the requirement $D_2 = D_1 + Q$, so the function will be continuous. On the first segment there is a shifted Morse potential, so under small displacements, the molecule's behavior is similar to the behavior under standard Morse potential. The third segment is an inverted Morse potential, and it serves as the repulsive potential at the decomposed state. The role of the polynomial in the intermediate segment is to link between the two edge segments. Therefore, the coefficients c_0, c_1, c_2, and c_3, are chosen to make the function and its first derivative continuous.

We determined the polynomial coefficients by the requirements for continuity of the potential and its first derivative at the points $r_{\min}$ and r_{bar} (the derivative vanishes at these points). There are four requirements, so the coefficients are determined uniquely. Using $Q = 1.5$ eV and $D_1 = 0.25$ eV (and, consequently, $D_2 = 1.75$ eV), and using Å as the length unit, we got $c_3 = -7.8125$, $c_2 = 39.8437$, $c_1 = -66.7969$, and $c_0 = 38.4141$, with the appropriate units. One can see that we can obtain continuity of the second derivative as well, by choosing $\beta_1 = \sqrt{3}/(r_{\text{bar}} - r_{\min}) = 4.3301$ Å^{-1} and $\beta_2 = \beta_1\sqrt{D_1/D_2} = 1.6366$ Å^{-1}. However, this is not essential, since the actual calculations during the simulations were done using cubic spline interpolation. This interpolation guarantees continuity of the second derivative.

For other exothermicity values (i.e., different Q), we used the same functional form on the first and second segments, with the same parameters' values, except Q and c_0, which determine the exothermicity. On the third segment, we determined the potential values in a way that maid only little gap of the function at r_{cut}. We also constructed potentials with different values for the barrier energy, using the same method.

APPENDIX C: CRYSTAL CHARACTERIZATION

Before shock propagations are examined the equilibrium structure and characteristics has to be determined. This was carried out by evaluating the position correlation function at different temperatures. In addition, the acoustical sound velocity was calculated.

1. Stability and phase transition temperature

Equilibrium *NPT* molecular dynamics simulations were performed under constant pressure of 1 bar, and at different temperatures. Under these conditions the stability of the N-C molecules as well as the stability of the crystal and its melting point were evaluated.

We found that the molecules are stable in the temperature range between 0 °K and 250 °K. When the temperature was raised beyond 250 °K, some of the N-C bonds started to dissociate. This is consistent with the low dissociation barrier of the molecule under examination, which is 0.25 eV.

The radial distribution functions (RDFs) of the N-N pairs were calculated. The results of the calculations for 50 °K and 250 °K are shown in Fig. 14. The observed peaks are in positions reflecting the FCC lattice. The RDFs verify that the crystal is solid up to 250 °K. As the temperature is raised from 50 °K to 250 °K, The peaks of the RDFs get broadened, and at 250 °K the RDF does not vanish after the third peak, as a result of large fluctuations.

On higher temperature, at 500 °K, some of the molecules decompose and the slab melts. The RDF of the system at this temperature shows liquid behavior. In Fig. 15 there is a plot of the RDF of N-N pairs on 500 °K. There are no sharp peaks at distances greater than the distance of the first nearest-neighbors peak. This character of the RDF is typical for the liquid phase.

2. Elastic sound velocity

a. The elastic sound velocity of our crystal

The MD simulation was used to determine velocity of the pressure p-wave in the crystal. A small longitudinal displacement of few crystal layers along the [111] direction was used to induce these waves. The perturbation propagation velocities was then determined. In order to ensure that the

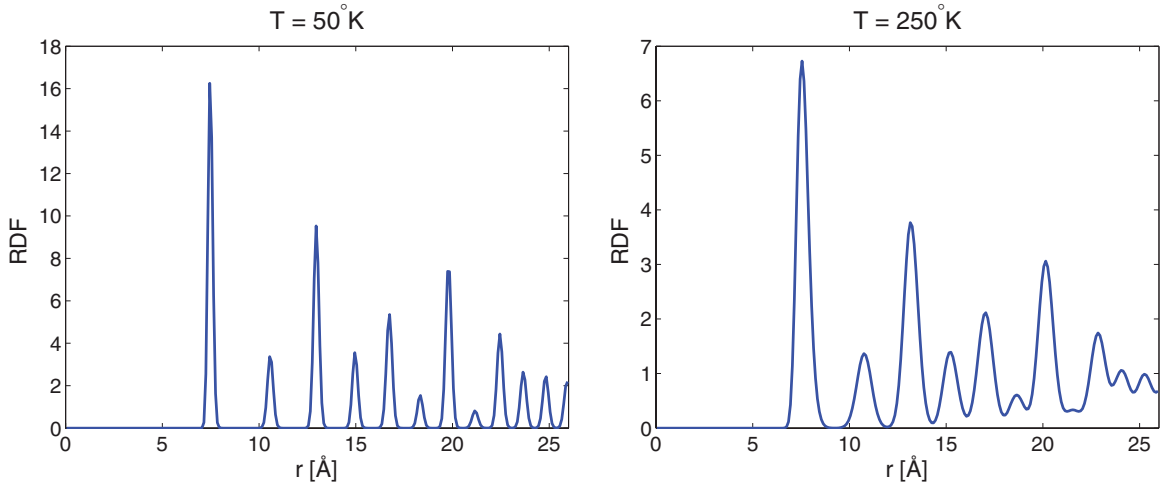

FIG. 14. (Color online) Radial distribution function of the crystal. Results are of a NPT simulations with 504 molecules at pressure of 1 bar. The left plot corresponds to 50 °K, and the right plot corresponds to 250 °K.

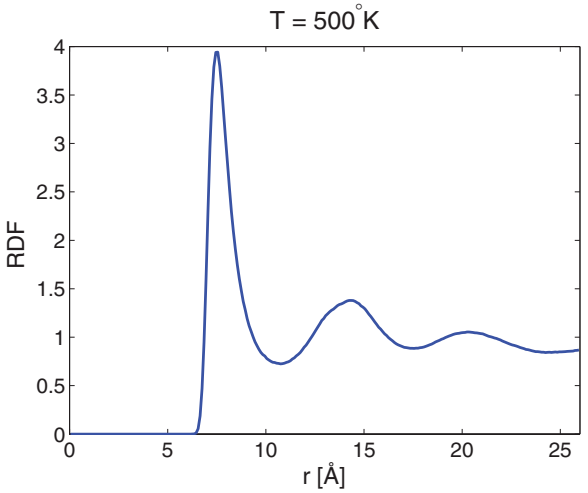

FIG. 15. (Color online) Radial distribution function of a NPT simulations with 504 molecules at pressure of 1 bar and temperature of 500 °K.

displacements are small enough, the simulations were repeated with various displacement amplitudes. It was then verified that the propagation velocity is independent of the displacement amplitude. We found that the p-wave velocity is approximately 2.6 unit cells per picosecond ($\approx 4.6\times 10^3$ m/s).

b. P-waves velocity on Morse crystals: A discussion

A simple 1D model may give an insight regarding the p-wave velocity in crystals for which the pair interaction is described by the Morse function. In this model there is an infinitely long chain of masses. Let us consider first an infinite harmonic chain. In this case the interaction between neighboring masses is harmonic, with a spring constant α. We

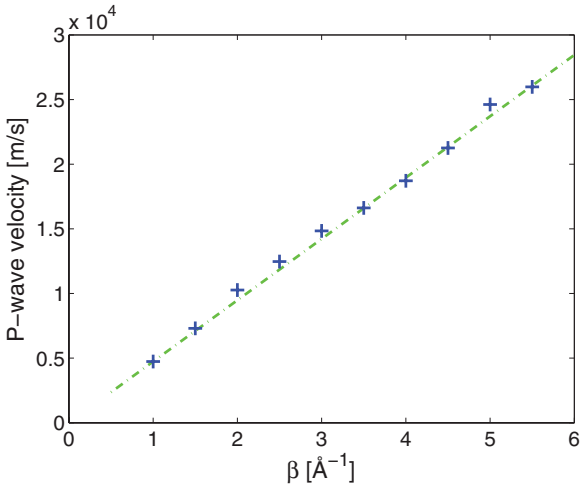

FIG. 16. (Color online) p-wave velocity in the crystal as a function of the β parameter in the intermolecular Morse potential. Each velocity was calculated by simulating propagation of small displacements in a crystal, with the relevant β parameter, and marked in the figure by a cross. The dashed line is an extrapolation to small β values assuming linear scaling.

denote the distance between two neighboring masses l. The equation of motion for the nth mass is

$$m\ddot{x}_n = \alpha(x_{n+1} - 2x_n + x_{n-1}). \tag{C1}$$

If we assume that the time-dependent position is given by

$$x_n(t) = (A_+ e^{+iknl} + A_- e^{-iknl})\cos(\omega t + \phi), \tag{C2}$$

we get the dispersion relation:

$$\omega(k) = 2\omega_0 \sin\left(\frac{kl}{2}\right), \tag{C3}$$

where we defined $\omega_0 = \sqrt{\alpha/m}$. The p-wave velocity for this case is

$$v_s = \left.\frac{d\omega}{dk}\right|_{k=0} = \omega_0 l \cos\left(\frac{kl}{2}\right)\Big|_{k=0} = \omega_0 l = \sqrt{\frac{\alpha}{m}}\, l. \tag{C4}$$

This model can be used to describe the harmonic approximation of small vibrations around the equilibrium distance

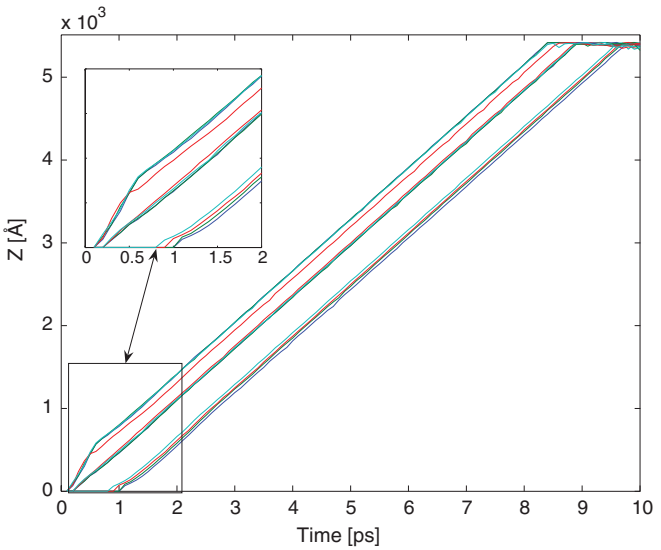

FIG. 17. (Color online) Reaction front location versus time in simulations with three different initial velocities of the pellet. The location was determined by a significant dissociation ratio. The results are grouped in three categories: The rightmost bundle represents five different simulations with the lowest pellet velocity used ($\approx$10 km/s). The central bundle corresponds to simulations (five runs) with medium pellet velocity ($\approx$50 km/s), while the leftmost bundle corresponds to simulations with the largest pellet velocity ($\approx$120 km/s). (These high values of initial velocities are used for demonstration: pellet velocities of 10, 50, and 120 km/s give rise to initial transient shock waves that are, respectively, slower, similar, and higher than the developing stable detonation wave, which is approximately 65 km/s. Smaller values of pellet velocities were used throughout most of this paper.) The different simulations in each one of the three groups correspond to different initial conditions used (slightly different initial pellet-crystal distance). A short time after the pellet collision with the slab, different shock wave velocities develop in each simulation. The differences between the trajectories at short times are shown in the insert of the figure. A stable, steady-state, velocity is reached after an additional propagation period. The shock velocity depends only on crystal parameters, which are identical in all simulations.

in the Morse potential (and other potentials). If the vibration amplitude is small enough for the harmonic approximation to hold, the propagation velocity of small perturbations should be independent of the perturbation amplitude. In such cases, we substitute $\alpha = 2\beta^2 D$, the second derivative near the minimum of the potential. Now the p-wave velocity is

$$v_s = \sqrt{\frac{\alpha}{m}} l = \sqrt{\frac{2D}{m}} \beta l. \tag{C5}$$

This result suggests that the p-wave velocity scales linearly with β.

The p-wave velocity in this simple 1D model is not directly comparable to the p-wave velocity in the 3D fcc slab, since the elastic waves on anisotropic crystal is determined by the elastic tensor σ, which has several parameters [54]. However, some insights can be gained: The MD simulation was employed to evaluate the p-wave velocity along the [111] direction of our slab. The assumption of the velocity's linear scaling as a function of β is tested by simulating propagation of small displacements in different crystals, while changing β. The results are shown in Fig. 16, marked by crosses. The dashed line in this figure is an extrapolation of the $\beta = 1$ case, assuming linear scaling. We can see that our assumption is valid in a wide range of the β values.

APPENDIX D: THE TRANSITION TO STATIONARY DETONATION WAVES

A stable detonation wave is independent of initial conditions. To check this hypothesis different initial pellet velocities were tested. The location of the reaction front was defined as the first point where molecular decomposition is identified. Figure 17 shows the location of the reaction front as a function of time in simulations with three different initial pellet velocities. Inspection of these results shows that a short time after the pellet collision with the slab, different shock wave velocities develop in each simulation. This is a transient: A stable, steady-state, velocity is reached after a short additional propagation period. The steady-state shock velocity depends only on crystal parameters. Therefore, it is clear that the pressure wave induced by the pellet in this model crystal develops into a constant velocity detonation wave. A similar transition from initiation dependent velocity to a steady-state velocity that depends only on crystal parameters was previously reported [55].

[1] W. Fickett and W. C. Davis, *Detonation: Theory and Experiment* (Dover Publication, Mineola, NY, 2000).

[2] J. A. Zukas and W. P. Walters, *Explosive Effects and Applications* (Springer-Verlag, New York, 2002).

[3] A. N. Dremin, *Toward Detonation Theory* (Springer-Verlag, New York, 1999).

[4] M. Ben-Artzi and J. Falcovitz, *Generalized Riemann Problems in Computational Fluid Dynamics* (Cambridge University Press, Cambridge, 2003).

[5] Ya. B. Zel'dovich, Zh. Eksp. Teor. Fiz. **10**, 542 (1940).

[6] J. Von Neumann, in *John von Neumann, Collected Works*, edited by A. J. Taub, Vol. 6 (Permagon Press, New York, 1963), pp. 178–202.

[7] W. Döring, Ann. Phys. **435**, 421 (1943).

[8] Ya. B. Zel'dovich, J. Exp. Theor. Phys. **12**, 389 (1942).

[9] C. M. Tarver, Combust. Flame **46**, 157 (1982).

[10] J. P. Chesick, J. Chem. Ed. **38**, 330 (1961).

[11] B. M. Rice, in *Modern Methods for Multidimensional Dynamics Computations in Chemistry*, edited by D. L. Thompson (World Scientific Publishing, New York, 1998), pp. 472–528.

[12] D. C. Sorescu, B. M. Rice, and D. L. Thompson, in *Energetic Materials, Part 1. Decomposition, Crystal and Molecular Properties*, edited by Peter Politzer and Jane S. Murray, *Theoretical and Computational Chemistry* 12 (Elsevier B.V., Amsterdam, 2003), pp. 125–184.

[13] D. W. Brenner, D. H. Robertson, M. L. Elert, and C. T. White, Phys. Rev. Lett. **70**, 2174 (1993).

[14] B. M. Rice, W. Mattson, J. Grosh, and S. F. Trevino, Phys. Rev. E **53**, 611 (1996).

[15] A. C. T. Van Duin, S. Dasgupta, F. Lorant, and W. A. Goddard III, J. Phys. Chem. A **105**, 9396 (2001).

[16] A. Strachan, A. C. T. van Duin, D. Chakraborty, S. Dasgupta, and W. A. Goddard, Phys. Rev. Lett. **91**, 098301 (2003).

[17] A. Strachan, E. M. Kober, A. C. T. van Duin, J. Oxgaard, and W. A. Goddard, J. Chem. Phys. **122**, 054502 (2005).

[18] F. Dubnikova, R. Kosloff, J. Almog, Y. Zeiri, R. Boese, H. Itzhaky, A. Alt, and E. Keinan, J. Am. Chem. Soc. **127**, 1146 (2005).

[19] A. C. T. van Duin, Y. Zeiri, F. Dubnikova, R. Kosloff, and W. A. Goddard, J. Am. Chem. Soc. **127**, 11053 (2005).

[20] W.-G. Liu, S. V. Zybin, S. Dasgupta, T. M. Klapoetke, and W. A. Goddard III, J. Am. Chem Soc. **131**, 22 (2009).

[21] A. C. Landerville, I. I. Oleynik, and C. T. White, J. Phys. Chem. A **113**, 12094 (2009).

[22] J. Budzien, A. P. Thompson, and S. V. Zybin, J. Phys. Chem. B **113**, 13142 (2009).

[23] S. V. Zybin, W. A. Goddard III, P. Xu, A. C. T. van Duin, and A. P. Thompson, Phys. Lett. A **96**, 081918 (2010).

[24] G. Stoltz, Europhys. Lett. **76**, 849 (2006).

[25] J. B. Maillet, L. Soulard, and G. Stoltz, Europhys. Lett. **78**, 68001 (2007).

[26] E. J. Reed, L. E. Fried, W. D. Henshaw, and C. M. Tarver, Phys. Rev. E **74**, 056706 (2006).

[27] M. Peyrard, S. Odiot, E. Lavenir, and J. Schnur, J. App. Phys. **57**, 2626 (1985).

[28] V. V. Zhakhovskiĭ, S. V. Zybin, K. Nishihara, and S. I. Anisimov, Phys. Rev. Lett. **83**, 1175 (1999).

[29] S. V. Zybin, V. V. Zhakhovskii, M. L. Elert, and C. T. White, AIP Conf. Proc. **706**, 310 (2004).

[30] J. Roth, Phys. Rev. B **72**, 014126 (2005).

[31] M. Toda, Suppl. Prog. Theor. Phys. **59**, 1 (1976).

[32] M. Toda, IEEE Trans. Circuits Syst. **30**, 542 (1983).

[33] B. L. Holian, H. Flaschka, and D. W. McLaughlin, Phys. Rev. A **24**, 2595 (1981).
[34] E. R. Dobbs and G. O. Jones, Rep. Prog. Phys. **20**, 516 (1957).
[35] A. J. Heim, N. Grnbech-Jensen, T. C. Germann, B. L. Holian, E. M. Kober, and P. S. Lomdahl, Phys. Rev. E **76**, 026318 (2007).
[36] V. Fomin, I. Golovnev, and A. Utkin, Shock Waves **15**, 325 (2006).
[37] M. L. Elert, J. J. C. Barrett, D. H. Robertson, and C. T. White, AIP Conf. Proc. **429**, 293 (1998).
[38] J. W. Dold and A. K. Kapila, Combust. Flame **85**, 185 (1991).
[39] T. J. Rolfe, S. A. Rice, and J. Dancz, J. Chem. Phys. **70**, 26 (1979).
[40] Ya. B. Zel'dovich, *Theory of Combustion and Detonation of Gases* (Akademiia Nauk SSSR, Moscow, 1944).
[41] A. N. Dremin, Combust. Explos. Shock Waves **36**, 704 (2000).
[42] C. S. Yoo, N. C. Holmes, P. C. Souers, C. J. Wu, F. H. Ree, and J. J. Dick, J. App. Phys. **88**, 70 (2000).
[43] M. W. Conroy, I. I. Oleynik, S. V. Zybin, and C. T. White, Phys. Rev. B **77**, 094107 (2008).
[44] M. W. Conroy, I. I. Oleynik, S. V. Zybin, and C. T. White, J. Phys Chem. A **113**, 3610 (2009).
[45] Ya. B. Zel'dovich, Combust. Flame **39**, 211 (1980).
[46] J. B. Bdzil and A. K. Kapila, Phys. Fluids A **4**, 409 (1992).
[47] A. K. Kapila, D. W. Schwendeman, J. J. Quirk, and T. Hawa, Combust. Theor. Model. **6**, 553 (2002).
[48] V. Balalaev, G. Dronin, and I. Veremeev Russian, J. Phys. Chem. B **2**, 172 (2008).
[49] M. Short and J. W. Dold, Combust. Theor. Model. **6**, 279 (2002).
[50] M. L. Elert, D. M. Deaven, D. W. Brenner, and C. T. White, Phys. Rev. B **39**, 1453 (1989).
[51] K. Refson, Comp. Phys. Comm. **126**, 310 (2000).
[52] D. Beeman, J. Comp. Phys. **20**, 130 (1976).
[53] M. P. Allen and D. J. Tildesley, *Computer Simulation of Liquids* (Oxford University Press, New York, 1989).
[54] J. M. Carcione, D. Kosloff, and R. Kosloff, Q. J. Mech. Appl. Math. **41**, 319 (1988).
[55] M. Peyrard, S. Odiot, E. Oran, J. Boris, and J. Schnur, Phys. Rev. B **33**, 2350 (1986).